Editors' Suggestion

Thickness-dependent topological spin texture nucleation in the high-temperature two-dimensional ferromagnet Fe_3GaTe_2

Y. Sun [1,*] M. T. Birch [2,†] D. A. Mayoh [3] Y. Liu [1] S. Satheesh [1] G. Balakrishnan [3] M. Weigand [4] S. Wintz [4] and M. Burghard [1,‡]

[1] Max Planck Institute for Solid State Research, Heisenbergstrasse 1, 70569 Stuttgart, Germany
[2] RIKEN Center for Emergent Matter Science (CEMS), Wako, Saitama 351-0198, Japan
[3] Department of Physics, University of Warwick, Coventry CV4 7AL, United Kingdom
[4] Helmholtz-Zentrum Berlin für Materialien und Energie GmbH, Institut Nanospektroskopie, 12489 Berlin, Germany

(Received 2 September 2025; revised 11 November 2025; accepted 29 January 2026; published 17 February 2026)

Fe_3GaTe_2 (FGaT) has emerged as a promising two-dimensional (2D) ferromagnet with intrinsic magnetism above room temperature. Here, we investigate the thickness-dependent nucleation and stability of topological spin textures in exfoliated FGaT flakes with thicknesses ranging from 45 to 290 nm using scanning transmission x-ray microscopy. The domain size exhibits a nonmonotonic dependence on thickness, deviating from classical Kittel's $t^{1/2}$ scaling due to enhanced domain-wall energy in thinner samples. Magnetic phase diagrams indicate that skyrmion nucleation becomes increasingly favorable with thickness, with a significantly expanded stability region in thicker flakes. In contrast, high-order spin textures are suppressed below ~75 nm, highlighting a critical limitation for the miniaturization of 2D skyrmion-based spintronic devices. Our results emphasize the need for better stabilization strategies, such as interfacial engineering in van der Waals heterostructures, to enable robust topological textures in thin 2D magnet flakes.

DOI: 10.1103/5nvm-zlgw

I. INTRODUCTION

The recently discovered two-dimensional (2D) van der Waals (vdW) ferromagnet Fe_3GaTe_2 (FGaT), exhibiting intrinsic ferromagnetism above room temperature [1], has enriched the rapidly evolving field of 2D magnetism, which began with the identification of ferromagnetism in layered $Cr_2Ge_2Te_6$ (CGT) [2] and CrI_3 [3]. In particular, FGaT has attracted considerable attention due to its elevated Curie temperature ($T_C = 350$–380 K) and strong perpendicular magnetic anisotropy that persists down to a few layers [4]. Remarkably, magnetic ordering is preserved down to the monolayer limit, with a T_C of approximately 345 K [5]. Similar to its sister compound Fe_3GeTe_2 (FGT), the properties of FGaT can be effectively tuned through proximity effects, strain engineering, and electrostatic doping in heterostructure devices [6–8]. Moreover, FGaT is a promising component of magnetic tunnel junctions (MTJs), magnetic random-access memory, and gate-tunable spin valves that can operate at ambient temperatures [9].

FGaT has been reported to host various types of topological spin textures, most prominently Néel-type skyrmions stable at room temperature and up to approximately 340 K with Fe intercalation into the vdW gap [10], as well as Bloch-type skyrmions that emerge along with hybrid skyrmions exhibiting mixed Bloch-Néel characteristics [11]. Notably, skyrmions remain stable at zero magnetic field over a wide temperature range [10,12]. It has been suggested that Néel-type skyrmion formation in FGaT is driven by a Dzyaloshinskii-Moriya interaction (DMI) resulting from defect- or vacancy-induced inversion symmetry breaking [13]. However, this interpretation remains a subject of debate. An alternative and potentially more plausible scenario posits that the skyrmions observed are actually Bloch type. In this view, the suggested Néel-type characteristics could arise due to the small domain-wall width, which may only become apparent under certain experimental conditions, such as when the sample is tilted. If bulk DMI were predominantly responsible, one would expect Néel-type skyrmions to be consistently observed even in thicker samples, which is not the case [14].

Besides skyrmions, higher-order topological spin textures such as skyrmioniums (topological charge $Q = 0$) and skyrmion bags ($Q \geqslant +1$ or $Q \leqslant -1$) have been observed [15], ascribed to Fe vacancy-induced local symmetry breaking and interfacial DMI [16]. Most recently, room-temperature twisted skyrmion bags, controllable by current pulses, and field-free sub-100-nm skyrmions writable by ultrafast femtosecond laser pulses have been observed, opening avenues for energy-efficient skyrmion-based logic and memory devices [16].

*Contact author: y.sun@fkf.mpg.de
†Contact author: maximilian.birch@riken.jp
‡Contact author: m.burghard@fkf.mpg.de

Thickness-dependent studies show larger skyrmions (∼180 nm diameter) in thicker flakes (>100 nm) stabilized by dipole-dipole interactions, while intermediate thicknesses (40−60 nm) host dense distributions (5−7 skyrmions/μm^2) with smaller diameters (∼90 nm) [17]. This finding has been attributed to an optimal balance between magnetic anisotropy and dipole interaction energies in this thickness regime. Notably, for Fe-deficient FGaT, the skyrmion size has been reported to decrease as sample thickness is reduced, with field-free sub-100-nm skyrmions obtainable at room temperature in samples thinner than 60 nm, achieving the smallest skyrmions reported in 2D vdW magnets and remaining stable over a broad temperature range (100−330 K), with the highest density observed with skyrmions sized between 46−60 nm [13]. These thickness-dependent variations in skyrmion size and density underscore the need for precise control over flake thickness to optimize topological spin textures for high-density, energy-efficient spintronic devices.

Here, we use scanning transmission x-ray microscopy (STXM) as a real-space imaging technique to directly visualize magnetic domains and topological spin textures in exfoliated FGaT sheets with thicknesses ranging from 45 to 290 nm, with the aim of determining comprehensive thickness-dependent magnetic phase diagrams. Crucially, our results reveal a thickness threshold of the order of 70–80 nm [atomic force microscopy (AFM)-measured thickness] below which the formation of high-order topological spin textures at room temperature (∼300 K) becomes increasingly challenging. In flakes thinner than this limit, large labyrinthine domains stabilize, consistent with theoretical predictions that account for finite-thickness effects beyond classical Kittel theory; upon further reduction in thickness, the system transitions to uniform magnetization reversal with a narrow temperature region for domains and skyrmions.

II. METHODS

Single crystals of Fe_3GaTe_2 were grown using the chemical vapor transport (CVT) method. Stoichiometric quantities of Fe powder, Ga pieces, and Te powder were inserted into a quartz tube. $TeCl_4$ was additionally added to the quartz tube at 1 mg/cm^3 to act as a transport agent before being sealed under vacuum. The tube was then heated in a two-zone furnace with the source temperature kept at 750 °C and the sink temperature kept at 700 °C. Once at temperature, this gradient was held for 7 days. The furnace was then allowed to cool back to room temperature. Magnetometry measurements on the bulk single crystals were carried out with a quantum design MPMS3 vibrating sample magnetometer. The magnetic properties were determined by aligning the crystal along the relevant crystal orientations (parallel and perpendicular to the c axis, respectively) and attaching it to a quartz glass rod using GE varnish. The built-in helium cryostat allowed temperature control down to 2 K while applying a magnetic field by a superconducting coil.

To prepare the FGaT flakes for the STXM experiments, the bulk crystal was first mechanically cleaved and then exfoliated onto a polydimethylsiloxane (PDMS) stamp. Suitable flakes were then stamped onto a 100-nm-thick Si_3N_4 membrane through proper control of mechanical forces at room temperature. The entire process was carried out under ambient conditions, with each side of the flake being exposed to the atmosphere for approximately 20 min. After stamping, the FGaT-coated membranes were immediately vacuum sealed to limit exposure to the environment, rather than capping them with hBN. FGaT flakes stamped under ambient conditions develop nonmagnetic surface-oxide layers of approximately 10 nm on each surface (about 20 nm total), as corroborated by the Fe $L_{2,3}$-edge x-ray absorption spectra in Fig. S2 in the Supplemental Material [18]. Flake thickness was determined with the aid of an atomic force microscope (Bruker dimension icon) operated in tapping mode. All thickness values reported in this paper are obtained directly from AFM measurements, without subtracting the ∼20 nm total contribution from the oxidized layers on both surfaces.

STXM experiments were performed at the end station at the BESSY II electron storage ring operated by the Helmholtz-Zentrum Berlin für Materialien und Energie [19]. This technique takes advantage of the synchrotron's tunable x-ray energy range to achieve element-specific chemical sensitivity, combined with nanoscale spatial resolution. By employing varying polarization states of the incident x-ray beam (left and right circular), x-ray magnetic circular dichroism (XMCD) measurements provide out-of-plane magnetization contrast specific to particular atomic species within the sample. STXM experiments were carried out at the Fe L_3 edge, with a nominal x-ray energy of 707.8 eV, utilizing an x-ray beam focused to approximately 25 nm spot size on the sample through a Fresnel zone plate (FZP) and an order selecting aperture (OSA). The FZP has a diameter of 320 μm with an outermost zone width of 18 nm. The sample was precisely positioned using a piezoelectric stage that enabled raster scanning through the focused beam. Temperature control was achieved using a He-flow cryostat, while the magnetic field was adjusted by reconfiguring four permanent magnets. Although the temperature was monitored by a sensor positioned near the sample, slight temperature differentials between sensor and sample may exist due to thermal coupling limitations. By recording the transmission signal pixel by pixel, we obtained spatial maps of the magnetic structure, with the measured signal indicating the out-of-plane magnetization (m_z). We present most of our data as single-helicity STXM images that contain both structural and magnetic contrast without additional processing. Single-helicity imaging preserves the structural context of magnetic domains relative to flake boundaries and eliminates drift-related artifacts inherent in difference imaging. Two different measurement protocols were used in the experiments. The field sweep (FS) method started by saturating the out-of-plane magnetization of the sample at a fixed temperature. STXM images were then systematically acquired, while the applied magnetic field was reversed in a stepwise manner. For the zero-field-cooling (ZFC) protocol, samples were first heated above their critical temperature and then cooled in the absence of an external magnetic field to achieve a controlled initial state. STXM images were then acquired during sequential field adjustments in both the positive and negative directions. Crucially, separate cooling cycles were required for each field sweep orientation to ensure consistent results.

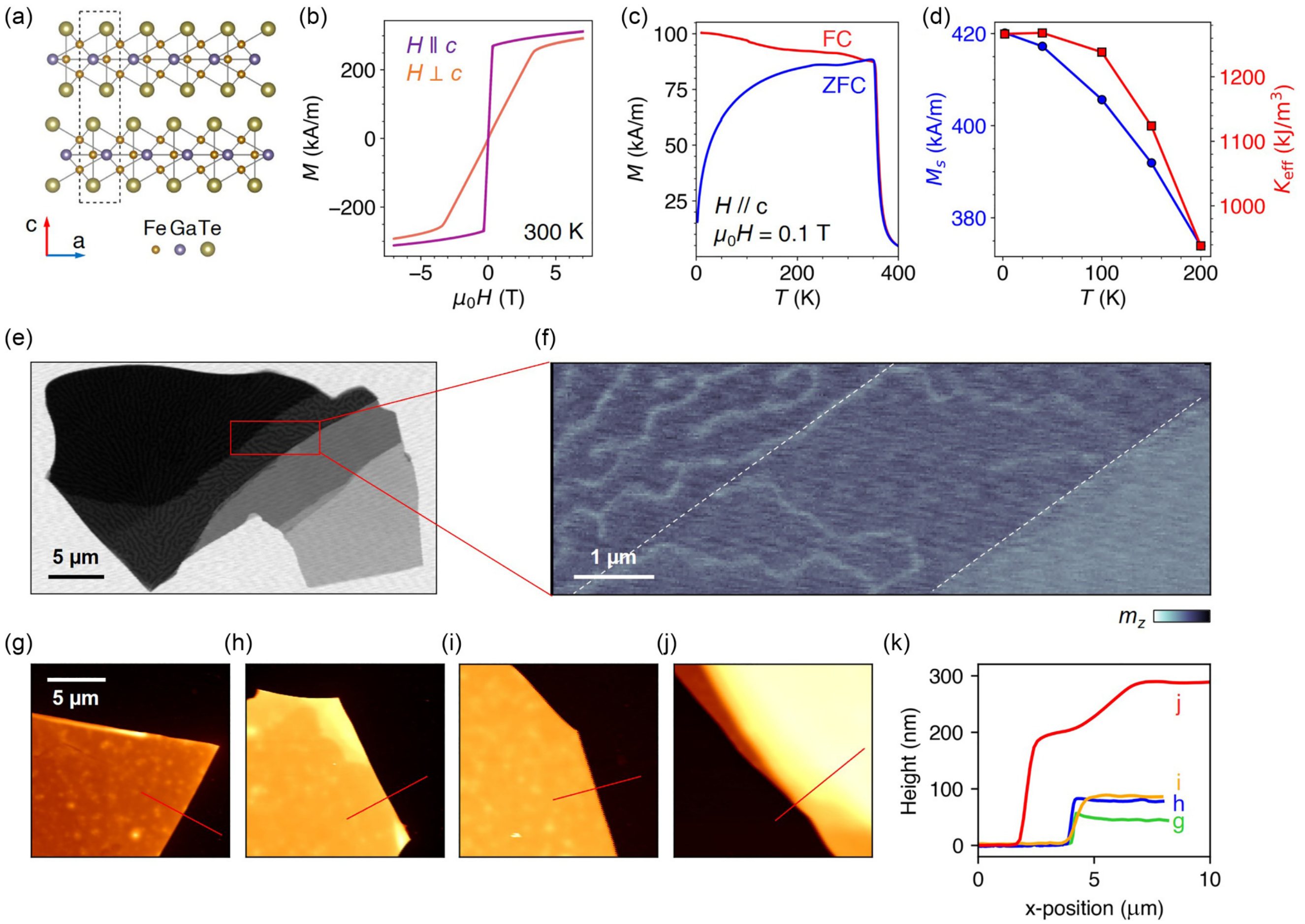

FIG. 1. Magnetic characterization of Fe_3GaTe_2 (FGaT) bulk crystal and thickness determination of the investigated FGaT flakes. (a) Crystal structure of FGaT viewed along the *b* axis. (b)–(d) Results of bulk SQUID magnetometry measurements including (b) hysteresis curves at $T = 300$ K for magnetic field parallel (purple curve) and perpendicular (orange curve) to the crystallographic *c* axis, (c) magnetization vs temperature curves along the *c* axis, comparing between zero-field cooling (ZFC) and field cooling (FC) at 0.1 T along the *c* axis, and (d) temperature evolution of saturation magnetization M_s (blue) and magnetic anisotropy K_{eff} (red). (e) Scanning transmission x-ray microscopy (STXM) image of an exfoliated FGaT flake with cascading thickness. (f) STXM image of magnetic domain structures in the area indicated in (e). The gray scale represents the out-of-plane magnetization component (m_z). (g)–(j) Atomic force microscopy (AFM) images of the four examined FGaT flakes, with red lines indicating the profile directions. (k) Section profiles corresponding to the AFM images in (g)–(j).

III. RESULTS

A. SQUID magnetometry

The layered crystal structure of FGaT is shown in Fig. 1(a), viewed along the crystallographic *b* axis. Magnetic hysteresis curves were recorded at 300 K using superconducting quantum interference device (SQUID) magnetometry, with the external magnetic field applied both parallel ($H \parallel c$) and perpendicular ($H \perp c$) to the crystallographic *c* axis [Fig. 1(b)]. The pronounced difference between these two orientations confirms that the easy axis of magnetization lies along the *c* axis, indicative of strong perpendicular magnetic anisotropy (PMA). ZFC and field-cooled (FC) magnetization measurements, performed under a 0.1 T magnetic field applied parallel to the *c* axis, reveal a sharp ferromagnetic-to-paramagnetic transition near 357 K [Fig. 1(c)], consistent with previous reports on FGaT [20]. The bifurcation between the ZFC and FC curves at low temperature is characteristic of ferromagnetic systems and suggests the formation of a multidomain magnetic state [21,22].

The saturation magnetization M_s, determined from hysteresis loops measured at various temperatures under fields applied parallel to the *c* axis, exhibits a monotonic decrease with increasing temperature, as shown in Fig. 1(d) (blue data points). At 2 K, M_s reaches 420 kA/m, corresponding to a magnetic moment of approximately 3.4 μ_B per Fe, calculated using the unit-cell volume of 2.23×10^{-28} m^3 and 3 Fe atoms per unit cell [5]. To quantitatively evaluate the thermal evolution of M_s, we analyzed temperature-dependent magnetization data by fitting it to a modified Bloch law, expressed as $M_s(T) = M_0(1 - BT^\alpha)$, where M_0 represents the saturation magnetization at 0 K, B is the Bloch coefficient, and α is the temperature exponent. The fitting procedure yielded an exponent of $\alpha \approx 1.7$, which is slightly higher than the classical value of 1.5 predicted by conventional spin-wave theory for 3D ferromagnetic systems [23]. Similar to other vdW magnets such as CrI_3 [24], the proximity of α to the 3D limit suggests that magnetic excitations in FGaT retain a pronounced 3D character at low temperatures despite its layered vdW

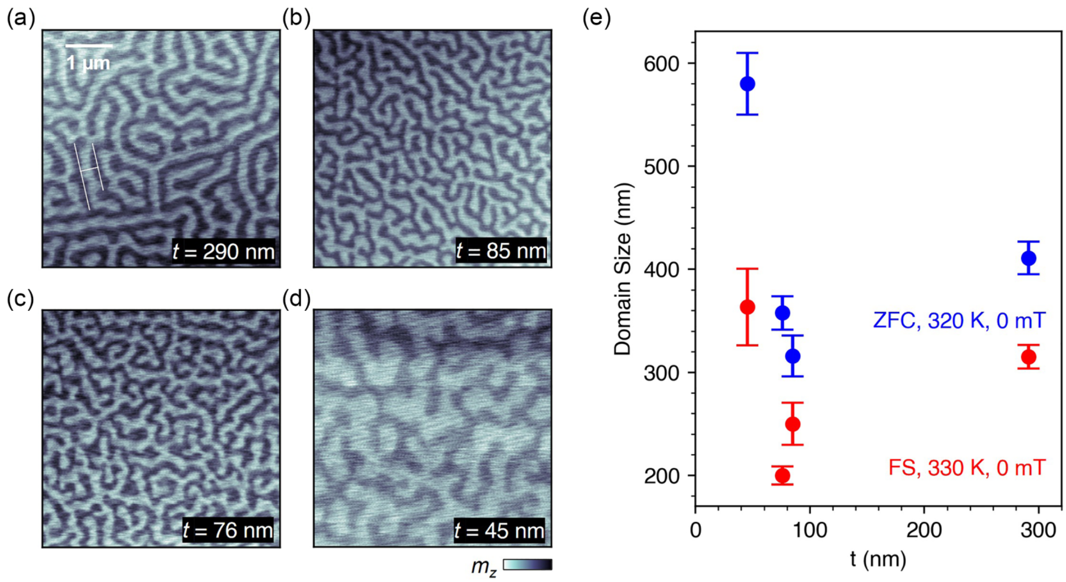

FIG. 2. Thickness-dependent magnetic domain structures in FGaT. (a)–(d) STXM images taken at $T = 320$ K of flakes of the indicated thickness. The contrast represents the out-of-plane magnetization component (m_z) as indicated by the gray scale. (e) Plot of magnetic domain size as a function of flake thickness measured under zero-field cooling (ZFC) at 320 K (blue data points) and field sweep (FS) at 330 K (red data points) conditions, both at zero magnetic field.

structure. The elevated α value likely originates from a thermally induced reduction in exchange splitting within the itinerant electron bands, which is characteristic of materials with strong electron correlations and itinerant magnetism [23,25].

The effective magnetic anisotropy K_{eff}, extracted from the difference between the in-plane and out-of-plane hysteresis loops [26], is also plotted in Fig. 1(d) (red data points). Classical theories generally predict a continuous, monotonic decrease in anisotropy with temperature [27]. Our results for FGaT are consistent with such trend, but reveal a two-regime behavior: K_{eff} remains relatively stable up to ~100 K and then decreases more rapidly at higher temperatures. The abrupt drop in K_{eff} is attributed to enhanced thermal fluctuations disrupting the orbital contributions to anisotropy. This likely occurs through modifications in the Fe-d orbital occupancy or crystal-field symmetry, which are pivotal for determining the magnetocrystalline anisotropy [28]. Indeed, the robust PMA in FGaT originates from distorted Fe octahedra within its crystal lattice, inducing strong crystal-field splitting of the Fe-d_{z^2} orbital. As the temperature increases above 100 K, thermal fluctuations increasingly disrupt this orbital order, leading to a ~75% reduction in K_{eff} by 200 K. This pronounced temperature sensitivity of PMA in FGaT contrasts with Cr-based vdW magnets such as CGT, where K_{eff} decreases by only 20% between 2 K and T_C [26]. Nevertheless, the sizable magnetic anisotropy ($K_{\mathrm{eff}} \approx 938$ kJ/m^3) retained at 200 K highlights the robust magnetic character of FGaT [4].

B. Thickness-dependent magnetic domains

To investigate the influence of thickness on the magnetic domain structure of FGaT, we mechanically exfoliated and characterized a series of flakes with varying thicknesses. Figure 1(e) displays a STXM image of a representative FGaT flake, exhibiting distinct regions with cascading thicknesses. The magnetic contrast image in Fig. 1(f), corresponding to the red-highlighted region in Fig. 1(e), reveals well-defined, stripelike magnetic domains in regions with thicknesses of 72, 56, and 19 nm, respectively (from left to right). The domain morphology and density vary noticeably across the different thickness regions, indicating a strong correlation between flake thickness and spin-texture formation.

To quantify the thickness of the investigated flakes, we performed atomic force microscopy (AFM). Figures 1(g)–1(j) present AFM images of four additional FGaT flakes, with red lines indicating the line scan paths. The corresponding height profiles in Fig. 1(k), extracted along these paths, confirm flake thicknesses t of 45 nm [Fig. 1(g)], 76 nm [Fig. 1(h)], 85 nm [Fig. 1(i)], and 290 nm [Fig. 1(j)].

1. Dependence of domain size on flake thickness

Figures 2(a)–2(d) display STXM images of the four FGaT flakes with varying thicknesses, captured under ZFC conditions at 320 K and zero field. These images reveal thickness-dependent magnetic domain structures. At intermediate thicknesses [$t = 85$ nm and $t = 76$ nm, Figs. 2(b) and 2(c)], labyrinthine domain patterns are observed, with domain sizes of approximate 350 nm. In the thickest flake [$t = 290$ nm, Fig. 2(a)], similar labyrinthine patterns persist, but the domain size increases to ~400 nm, consistent with the reduced domain density observed in thicker flakes [17]. Conversely, the thinnest flake [$t = 45$ nm, Fig. 2(d)] exhibits significantly larger domains, indicating a shift in the dominant magnetic anisotropy as thickness decreases.

Figure 2(e) quantifies this behavior, plotting average domain size against thickness under ZFC (blue data points) and FS (red data points) conditions, both at zero external magnetic field. Importantly, the similar trend observed for both protocols at different temperatures (320 K and 330 K) demonstrates that the nonmonotonic thickness dependence is robust and independent of measurement protocols and small temperature variations. The domain size exhibits a nonmonotonic trend: it decreases with increasing thickness up to ∼100 nm, where it reaches a minimum, and then increases for thicker flakes. This trend deviates from Kittel's law, which predicts domain size l scales as $l \propto t^{1/2}$ due to a balance between domain-wall energy (favoring larger domains) and magnetostatic energy (favoring smaller domains to reduce stray fields) [29]. While intermediate and thicker flakes align roughly with this scaling, the anomalously large domains in the 45 nm flake suggest a breakdown of Kittel's assumptions in the thin regime. This deviation reflects that in the thin-film limit, the domain-wall energy, defined by the exchange stiffness A and the effective perpendicular anisotropy K_{eff}, outweighs the magnetostatic (dipolar) energy. Thin-film micromagnetic models [30,31] therefore predict that the system minimizes its total energy by suppressing domain-wall density, resulting in very large-period labyrinthine (or even quasi-uniform) states rather than a dense stripe pattern. An analytically improved, revised Kittel-type model [31] treats the magnetostatic energy using a full Fourier-space evaluation of the demagnetizing field for finite-thickness, finite-period domains, rather than the long-wavelength approximation of the classical Kittel law. This framework predicts a nonmonotonic dependence of the domain size, i.e., l first decreases as thickness t increases from the ultrathin limit, reaches a minimum at an intermediate, sample-dependent crossover thickness (∼100 nm in the present flakes), and then increases again for thicker flakes. In the thin limit ($t \ll l$), magnetostatic energy per unit area is strongly suppressed (it scales roughly with the film thickness), whereas the domain-wall energy per unit area remains substantial. The film therefore lowers its total energy by tolerating higher stray-field cost in exchange for fewer walls, yielding comparatively large domains. Near the crossover thickness, the wall energy and dipolar energy balance, producing the smallest observed l. For $t \gg l$, dipolar interactions dominate and drive an increase of l to improve flux closure, approaching the asymptotic Kittel-like scaling $l \propto t^{1/2}$ that is characteristic of magnetostatically dominated thick films [29].

2. Thickness dependence of skyrmion nucleation

To systematically explore the nucleation and stability of skyrmions in FGaT, we performed FS STXM measurements at various temperatures across three of the flakes, with thicknesses of 45 nm, 76 nm, and 290 nm (Fig. S4 in the Supplemental Material [18]). Starting from negative magnetic saturation, we tracked the magnetic texture evolution under increasing out-of-plane field at each temperature. Across all thicknesses, the general progression follows a typical PMA material sequence, i.e., from saturated magnetization to stripe domains (SDs) to skyrmions (Sk), before reentering saturation at positive fields [32].

In the thinnest flake (45 nm), at 320 K, the magnetization reverses uniformly without the formation of domains (Fig. S4(a) in the Supplemental Material [18]). Upon increasing the temperature to 335 K, stripe domains begin to emerge as the field approaches zero, indicating the onset of domain instability (Figs. S4(b) and S4(c) in the Supplemental Material [18]). However, at 340 K, no magnetic domains are detected, suggesting that this temperature exceeds T_C for this particular thickness and the sample becomes paramagnetic (Fig. S4(d) in the Supplemental Material [18]). For the intermediate thickness (76 nm), stripe domains are more prominent, and the field window over which these domains are stable expands as the temperature increases from 320 K to 340 K (Figs. S4(e)–S4(h) in the Supplemental Material [18]). This indicates enhanced domain stability and a broader coexistence region of stripe and skyrmion phases in thicker flakes. Similarly, the thickest flake (290 nm) exhibits well-developed labyrinthine domain patterns at lower fields which evolve into wormlike structures as the field increases (Figs. S4(i)–S4(l) in the Supplemental Material [18]). Clear skyrmion formation is evident at the highest investigated temperature of 340 K (Fig. S4(l) in the Supplemental Material [18]). In summary, while skyrmions can form in all three thicknesses under appropriate conditions, their nucleation becomes increasingly favorable with thickness, i.e., occurring only transiently in the 45 nm flake near T_C, across broader parameter windows in the 76 nm flake, and predominantly at elevated temperatures in the 290 nm flake. This demonstrates that increased thickness not only stabilizes complex domain textures, but also facilitates the nucleation of skyrmions at elevated temperatures.

Taken together, these observations demonstrate that thickness plays a critical role in enabling skyrmion nucleation under FS protocols. Our observation of skyrmions already at a flake thickness as small as ∼45 nm is in contrast to the recent report by Jin *et al.* of skyrmion formation in FGaT above ∼150 nm [17]. However, it is important to note that they used a FC protocol, while our results show that a FS protocol can nucleate skyrmions also in thinner flakes, provided the system is near T_C, where thermal fluctuations flatten the magnetic energy landscape and allow metastable topological textures to emerge. Additionally, small differences in the Fe content of the samples may contribute to this discrepancy. The thickness-dependent trend observed in Fig. S4 in the Supplemental Material [18] is consistent with Bloch-type ("bubble") behavior stabilized by dipolar interactions and is not easily explained by a purely defect-induced DMI scenario [13]. In thicker flakes, the larger stray-field (demagnetizing) energy makes it energetically favorable to form localized bubble/skyrmion domains during the field sweep, whereas thinner flakes either reverse nearly uniformly or only transiently form broad stripes.

3. Thickness-dependent magnetic phase diagrams

A comprehensive analysis of FS STXM images of the different flakes, acquired as a function of both applied field and temperature, enabled the construction of detailed magnetic phase diagrams, as presented in Fig. 3. These phase diagrams reveal a rich landscape of magnetic states, particularly near T_C where stripe domains and skyrmions emerge and often coexist.

A clear trend is observed as the flake thickness increases: the stability region of the skyrmion phase (depicted in green) expands significantly. For the thinnest flake

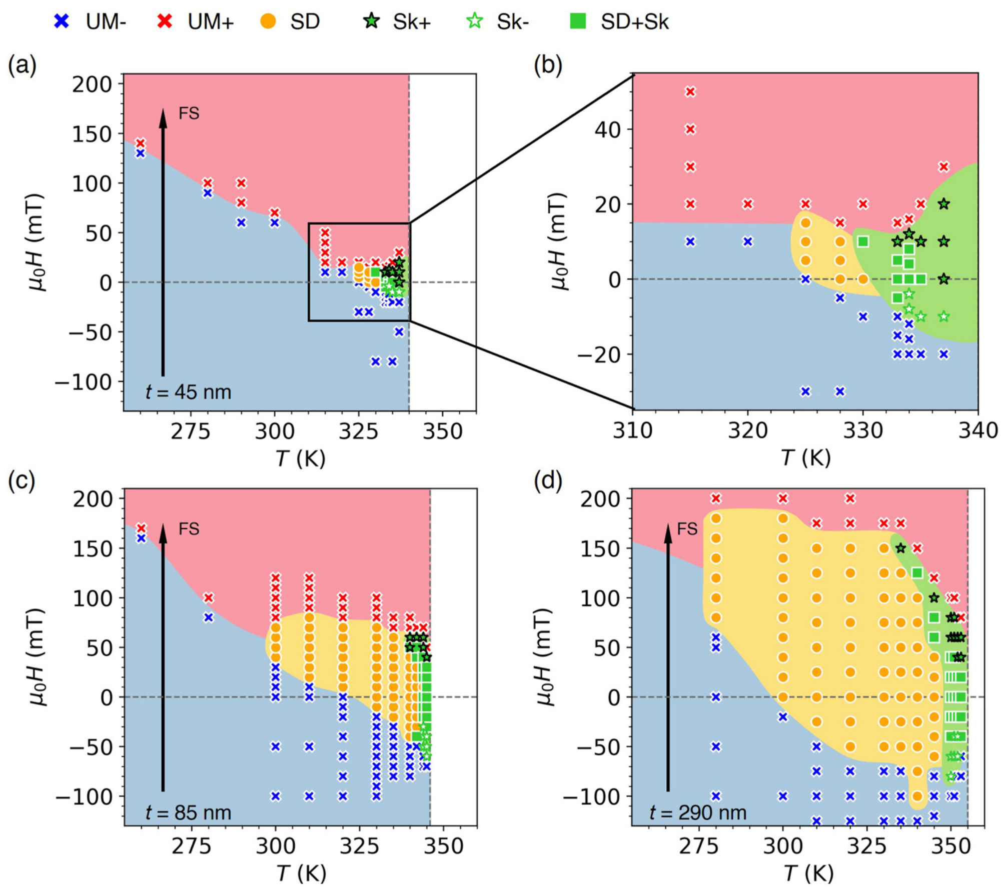

FIG. 3. Magnetic phase diagrams of the different FGaT flakes, as determined from STXM images. (a) Phase diagram for the thinnest flake (45 nm). (b) Magnified view of the region marked in (a), highlighting the phase transitions in vicinity of T_C. (c),(d) Phase diagram of the (c) 85-nm-thick flake and (d) 290-nm-thick flake. The different magnetic states are labeled as follows: uniformly magnetized states with negative (UM-, blue x's) and positive (UM+, red x's) magnetization, stripe domain state (SD, orange circles), skyrmions in positive (Sk+, green-filled black stars) and negative (Sk−, empty green stars) external magnetic field, and coexisting stripe domains and skyrmions (SD + Sk, green squares). The vertical arrows indicate the FS direction. The vertical dashed lines mark the Curie temperature for each flake.

[Figs. 3(a) and 3(b)], skyrmions (Sk) appear only within a narrow field window, approximately from −10 mT to 30 mT. In contrast, for the thicker flakes [Figs. 3(c) and 3(d)], the skyrmion phase extends over a much broader field range, extending from about −80 mT to 150 mT in the thickest sample. This pronounced broadening reflects a substantial enhancement in skyrmion stability with increasing thickness. The stripe domain (SD) phase (yellow) similarly expands in both field and temperature range with increasing flake thickness. Moreover, coexisting SD and Sk phases are observed over extended field intervals, indicative of a metastable regime where multiple magnetic configurations are energetically competitive.

The evolution of magnetic phases with thickness reflects the same competition between perpendicular anisotropy and dipolar interactions discussed above. Overall, the magnetic phase diagrams highlight flake thickness as a key tuning parameter for controlling the topology and stability of spin textures in FGaT.

4. Nucleation of higher-order topological spin textures

Having discussed the dependence of skyrmion nucleation on FGaT thickness, we now address the formation of higher-order topological spin textures, such as skyrmioniums and skyrmion bags, which exhibit intricate magnetic configurations with distinct topological properties. To investigate their emergence, we analyzed the field evolution of magnetic domains after ZFC, as shown in Fig. 4. In the thickest FGaT flake [Figs. 4(a)–4(c)], a clear progression of magnetic domain structures is observed as the magnetic field increases from 100 mT to 175 mT. At 100 mT, labyrinthlike stripe domains dominate. As the field increases to 150 mT and further to 175 mT, domain walls become increasingly sparse and isolated magnetic objects begin to emerge. Notably, at 175 mT, skyrmioniums and skyrmion bags emerge, which corresponds to the regime where stripe domains collapse into isolated structures, as observed in magnetic domain studies of FGaT [33]. A similar trend is observed in the intermediate-thickness flake [Figs. 4(d)–4(f)], measured under fields from 25 mT to 110 mT. Dense stripes at 25 mT evolve into more isolated textures at 75 mT, and at 110 mT, nearly all domains vanish, with only three well-defined skyrmioniums remaining. In contrast, the thinnest flake [Figs. 4(g)–4(i)] shows no formation of higher-order textures. Although initial stripe domains are observed at 5 mT, they vanish entirely by 20 mT without transitioning into higher-order textures.

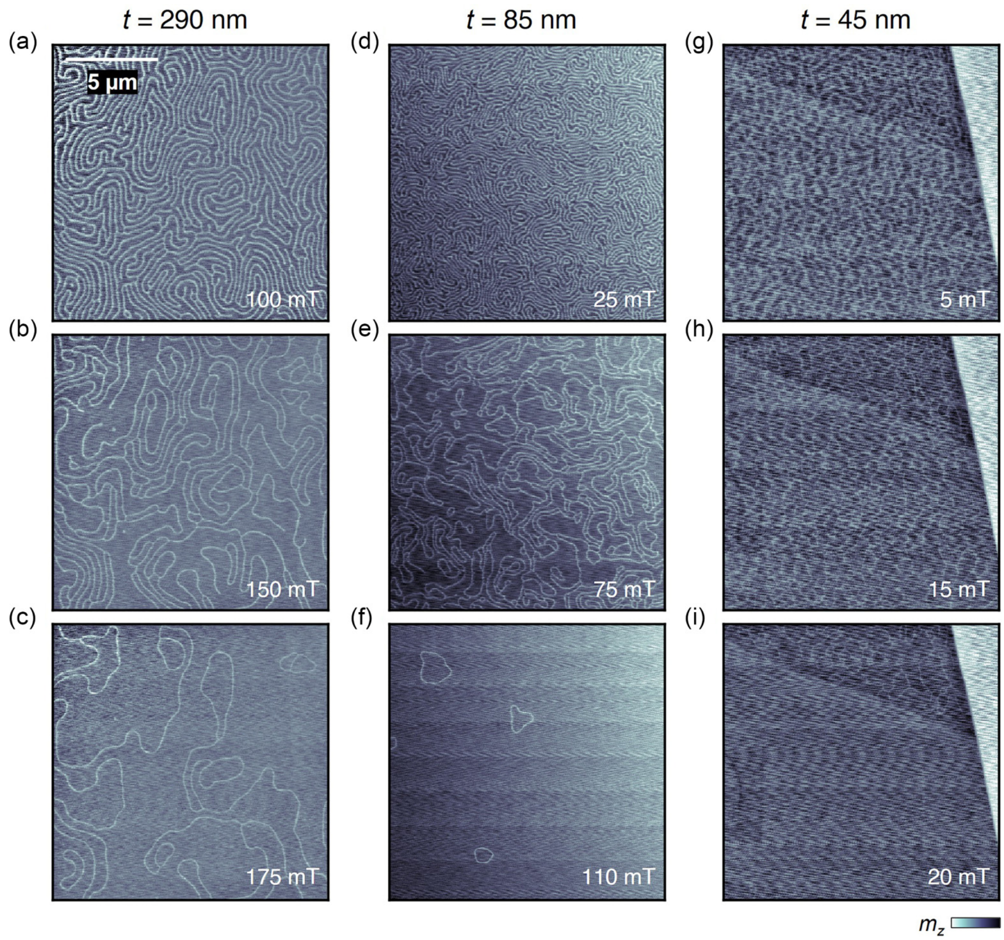

FIG. 4. STXM images illustrating the evolution of magnetic domains in the different FGaT flakes as a function of applied out-of-plane magnetic field after ZFC. All the images were acquired at 320 K. (a)–(c) Thickest flake displaying mazelike stripe domains that gradually transform as the field increases from 100 mT to 175 mT, with domain walls becoming less dense and more isolated at higher fields. At the highest field, the skyrmionium and skyrmion bag appear. (d)–(f) Intermediate-thickness flake featuring a similar evolution from 25 mT to 110 mT. At the highest field, almost all domains have disappeared, with the exception of three skyrmioniums. (g)–(i) Thinnest flake showing no formation of skyrmioniums or skyrmion bags under ZFC. Labyrinthine domains (g) appear at the lowest field of 5 mT, (h) become less dense at 15 mT, and (i) disappear entirely at 20 mT. The gray scale represents the out-of-plane magnetization component (m_z).

The fact that higher-order topological textures appear only in the two thicker flakes strongly supports the role of dipolar interactions in stabilizing these states. In thin flakes, where exchange and anisotropy dominate, the formation of curved or closed-loop domains is energetically unfavorable. This behavior parallels observations in other 2D ferromagnets, such as CGT, where skyrmioniums form only in sufficiently thick layers [26]. The nucleation protocol also plays a critical role. In our experiments, higher-order textures were observed exclusively under the ZFC protocol, while FS measurements failed to produce skyrmioniums or bags in any thickness. This distinction echoes results in FGT, where ZFC was shown to seed domain configurations favorable for skyrmionium formation [34]. Under ZFC, labyrinthine precursors act as closed-loop templates from which skyrmioniums can evolve. In contrast, during FS, repulsive domain-domain interactions likely introduce energetic barriers that prevent the formation of these complex textures.

IV. CONCLUSIONS

Using STXM, we systematically explored how flake thickness governs magnetic domain structure and the formation of topological spin textures in FGaT. Our results reveal that domain size depends nonmonotonically on thickness. The smallest domains are found at intermediate thicknesses, while much larger domains are found in the thinnest and thickest flakes. This deviates from classical Kittel scaling. The behavior reflects a crossover from domain-wall energy-dominated regimes in thin flakes to dipolar-dominated regimes in thicker samples. A key finding is the existence of a critical thickness threshold of ∼75 nm for stabilizing high-order topological spin textures, such as skyrmioniums and skyrmion bags. Their nucleation is also strongly protocol dependent, with ZFC being essential for stabilization.

Our findings underscore a significant challenge in the field of 2D magnetism, i.e., the uniaxial anisotropy that elevates

T_C and facilitates high-temperature magnetic ordering is the same property that suppresses the formation of domains and skyrmions in thinner samples. This presents a considerable obstacle for the development of domain-wall and skyrmion-based devices using 2D magnets in their thinnest form. For applications requiring dense arrays of topological spin textures, intermediate thicknesses (75−100 nm) offer an optimal balance between nucleation efficiency and stability. Thicker flakes (>200 nm) support more complex textures, including skyrmion bags, which may enable multibit data-encoding schemes. Conversely, flakes thinner than ∼75 nm exhibit uniform or large labyrinthine domains at room temperature, making them unsuitable for skyrmion-based device architectures. To overcome the observed thickness limitation for practical spintronic applications, strain engineering via, for instance, micropillars can enhance the Curie temperature and perpendicular magnetic anisotropy in FGaT, potentially enabling the formation of higher-order topological spin textures in thinner films [35]. Alternatively, interfacing ultrathin FGaT with high spin-orbit-coupling materials can induce interfacial Dzyaloshinskii-Moriya interactions (DMI) that provide additional chiral stabilization for topological spin textures, compensating for reduced dipolar interactions in thinner films [36].

ACKNOWLEDGMENTS

We thank the Helmholtz-Zentrum Berlin für Materialien und Energie for the allocation of synchrotron radiation beam time. Part of this work was supported by the Deutsche Forschungsgemeinschaft (DFG) priority program SPP2244 via Grant No. BU 1125/12-2. M.T.B. acknowledges the support of the RIKEN Special Postdoctoral Researcher scheme.

DATA AVAILABILITY

The data that support the findings of this article are not publicly available upon publication because it is not technically feasible and/or the cost of preparing, depositing, and hosting the data would be prohibitive within the terms of this research project. The data are available from the authors upon reasonable request.

[1] J.-E. Lee, S. Yan, S. Oh, J. Hwang, J. D. Denlinger, C. Hwang, H. Lei, S.-K. Mo, S. Y. Park, and H. Ryu, Electronic structure of above-room-temperature van der Waals ferromagnet Fe_3GaTe_2, Nano Lett. **23**, 11526 (2023).

[2] C. Gong, L. Li, Z. Li, H. Ji, A. Stern, Y. Xia, T. Cao, W. Bao, C. Wang, Y. Wang, Z. Q. Qiu, R. J. Cava, S. G. Louie, J. Xia, and X. Zhang, Discovery of intrinsic ferromagnetism in two-dimensional van der Waals crystals, Nature (London) **546**, 265 (2017).

[3] B. Huang, G. Clark, E. Navarro-Moratalla, D. R. Klein, R. Cheng, K. L. Seyler, D. Zhong, E. Schmidgall, M. A. McGuire, D. H. Cobden, W. Yao, D. Xiao, P. Jarillo-Herrero, and X. Xu, Layer-dependent ferromagnetism in a van der Waals crystal down to the monolayer limit, Nature (London) **546**, 270 (2017).

[4] A. M. Ruiz, D. L. Esteras, D. López-Alcalá, and J. J. Baldoví, On the origin of the above-room-temperature magnetism in the 2D van der Waals ferromagnet Fe_3GaTe_2, Nano Lett. **24**, 7886 (2024).

[5] S. Wu, Z. He, M. Gu, L. Ren, J. Li, B. Deng, D. Wang, X. Guo, W. Li, M. Chen, Y. Chen, M. Meng, Q. Ye, B. Shen, X. Chen, J. Guo, G. Xing, I. K. Sou, and S. Li, Robust ferromagnetism in wafer-scale Fe_3GaTe_2 above room-temperature, Nat. Commun. **15**, 10765 (2024).

[6] X. Guo, J. Li, W. Li, M. Chen, Q. Ye, S. Wu, and S. Li, Ferromagnetic enhancement of $Fe_3GaTe_2/PtTe_2$ induced by interfacial spin–orbit coupling, Appl. Phys. Lett. **126**, 102402 (2025).

[7] S. Jin, Y. Liu, Z. Deng, T. Wang, S. Xu, Y. Chen, X. Jiang, C. Liang, J. Hong, S.-W. Cheong, and X. Wang, Strain gradient induced skyrmion in a van der Waals magnet by wrinkling, Adv. Mater. **37**, 2501935 (2025).

[8] J. Han, B. Marfoua, and J. Hong, Strain-dependent magnetic properties of two-dimensional Fe_3GaTe_2, J. Magnet. **29**, 166 (2024).

[9] H. Pan, A. K. Singh, C. Zhang, X. Hu, J. Shi, L. An, N. Wang, R. Duan, Z. Liu, S. S. P. Parkin, P. Deb, and W. Gao, Room-temperature tunable tunneling magnetoresistance in $Fe_3GaTe_2/WSe_2/Fe_3GaTe_2$ van der Waals heterostructures, InfoMat **6**, e12504 (2024).

[10] R. Saha, H. L. Meyerheim, B. Göbel, I. Mertig, and S. S. P. Parkin, High-temperature Néel skyrmions in Fe_3GaTe_2 stabilized by Fe intercalation into the van der Waals gap, npj Spintron. **2**, 21 (2024).

[11] X. Lv, H. Lv, Y. Huang, R. Zhang, G. Qin, Y. Dong, M. Liu, K. Pei, G. Cao, J. Zhang, Y. Lai, and R. Che, Distinct skyrmion phases at room temperature in two-dimensional ferromagnet Fe_3GaTe_2, Nat. Commun. **15**, 3278 (2024).

[12] B. Ding, X. Li, Z. Li, X. Xi, Y. Yao, and W. Wang, Tuning the density of zero-field skyrmions and imaging the spin configuration in a two-dimensional Fe_3GeTe_2 magnet, NPG Asia Mater. **14**, 74 (2022).

[13] Z. Li, H. Zhang, G. Li, J. Guo, Q. Wang, Y. Deng, Y. Hu, X. Hu, C. Liu, M. Qin, X. Shen, R. Yu, X. Gao, Z. Liao, J. Liu, Z. Hou, Y. Zhu, and X. Fu, Room-temperature sub-100 nm Néel-type skyrmions in non-stoichiometric van der Waals ferromagnet $Fe_{3-x}GaTe_2$ with ultrafast laser writability, Nat. Commun. **15**, 1017 (2024).

[14] S. Xia, Y. Luo, I. A. Malik, X. Zhou, K. Han, Y. Sun, H. Lin, H. Shi, Y. Cheng, V. L. Zhang, Y. Du, S. Liu, C. Zhu, and T. Yu, Spontaneous enhancement of Dzyaloshinskii-Moriya Interaction via field-cooling-induced interface engineering in 2D van der Waals ferromagnetic ternary tellurides, arXiv:2505.06924v2.

[15] H. Zhang, Y.-T. Shao, X. Chen, B. Zhang, T. Wang, F. Meng, K. Xu, P. Meisenheimer, X. Chen, X. Huang, P. Behera, S. Husain, T. Zhu, H. Pan, Y. Jia, N. Settineri, N. Giles-Donovan, Z. He, A. Scholl, A. N'Diaye, *et al.*, Spin disorder control of topological spin texture, Nat. Commun. **15**, 3828 (2024).

[16] J. Jiang, Y. Wu, L. Kong, Y. Zhang, S. Qiu, H. Zhang, Y. Ke, S. Wang, M. Tian, and J. Tang, Stable Néel-twisted Skyrmion bags in a van der Waals magnet $Fe_{3-x}GaTe_2$ at room temperature, Nano Lett. **25**, 3282 (2025).

[17] S. Jin, Y. Wang, H. Zheng, S. Dong, K. Han, Z. Wang, G. Wang, X. Jiang, X. Wang, J. Hong, H. Huang, Y. Zhang, T.-L. Xia, and X. Wang, Thickness- and field-dependent magnetic domain evolution in van der Waals Fe_3GaTe_2, Nano Lett. **24**, 5467 (2024).

[18] See Supplemental Material at http://link.aps.org/supplemental/10.1103/5nvm-zlgw for the discussion of surface oxidation based on x-ray absorption spectra; SQUID measurements; domain-size calculations; contrast normalization; and additional data sets of the field sweep STXM images, which includes Refs. [32,37].

[19] M. Weigand, S. Wintz, J. Gräfe, M. Noske, H. Stoll, B. Van Waeyenberge, and G. Schütz, TimeMaxyne: A shot-noise limited, time-resolved pump-and-probe acquisition system capable of 50 GHz frequencies for synchrotron-based X-ray microscopy, Crystals **12**, 1029 (2022).

[20] C. Zhang, Z. Jiang, J. Jiang, W. He, J. Zhang, F. Hu, S. Zhao, D. Yang, Y. Liu, Y. Peng, H. Yang, and H. Yang, Above-room-temperature chiral skyrmion lattice and Dzyaloshinskii-Moriya interaction in a van der Waals ferromagnet $Fe_{3-x}GaTe_2$, Nat. Commun. **15**, 4472 (2024).

[21] M. Wang, B. Lei, K. Zhu, Y. Deng, M. Tian, Z. Xiang, T. Wu, and X. Chen, Hard ferromagnetism in van der Waals Fe_3GaTe_2 nanoflake down to monolayer, npj 2D Mater. Appl. **8**, 22 (2024).

[22] J.-j. Guo, Q.-l. Xia, X.-g. Wang, Y.-z. Nie, R. Xiong, and G.-h. Guo, Temperature and thickness dependent magnetization reversal in 2D layered ferromagnetic material Fe_3GeTe_2, J. Magn. Magn. Mater. **527**, 167719 (2021).

[23] Z. Fei, B. Huang, P. Malinowski, W. Wang, T. Song, J. Sanchez, W. Yao, D. Xiao, X. Zhu, A. F. May, W. Wu, D. H. Cobden, J.-H. Chu, and X. Xu, Two-dimensional itinerant ferromagnetism in atomically thin Fe_3GeTe_2, Nat. Mater. **17**, 778 (2018).

[24] Y. Liu and C. Petrovic, Three-dimensional magnetic critical behavior in CrI_3, Phys. Rev. B **97**, 014420 (2018).

[25] H. Wu, C. Hu, Y. Xie, B. G. Jang, J. Huang, Y. Guo, S. Wu, C. Hu, Z. Yue, Y. Shi, R. Basak, Z. Ren, T. Yilmaz, E. Vescovo, C. Jozwiak, A. Bostwick, E. Rotenberg, A. Fedorov, J. D. Denlinger, C. Klewe, *et al.*, Spectral evidence for local-moment ferromagnetism in the van der Waals metals Fe_3GaTe_2 and Fe_3GeTe_2, Phys. Rev. B **109**, 104410 (2024).

[26] L. Powalla, M. T. Birch, K. Litzius, S. Wintz, S. Satheesh, M. Weigand, E. Goering, G. Schütz, and M. Burghard, Skyrmion and skyrmionium formation in the two-dimensional magnet $Cr_2Ge_2Te_6$, Phys. Rev. B **108**, 214417 (2023).

[27] J. B. Staunton, L. Szunyogh, A. Buruzs, B. L. Gyorffy, S. Ostanin, and L. Udvardi, Temperature dependence of magnetic anisotropy: An *ab initio* approach, Phys. Rev. B **74**, 144411 (2006).

[28] L. Deng, X. Yin, J. Tong, Y. Wu, F. Tian, and X. Zhang, Writing and reading magnetization states via strain in Fe_3GaTe_2/h-BN/$MnBi_2Te_4$ junction, J. Appl. Phys. **135**, 174303 (2024).

[29] C. Kittel, Theory of the structure of ferromagnetic domains in films and small particles, Phys. Rev. **70**, 965 (1946).

[30] F. Virot, L. Favre, R. Hayn, and M. D. Kuz'min, Theory of magnetic domains in uniaxial thin films, J. Phys. D **45**, 405003 (2012).

[31] C. M. Teodorescu, Kittel's model for ferromagnetic domains, revised and completed, including the derivation of the magnetic hysteresis, Results Phys. **46**, 106287 (2023).

[32] M. T. Birch, L. Powalla, S. Wintz, O. Hovorka, K. Litzius, J. C. Loudon, L. A. Turnbull, V. Nehruji, K. Son, C. Bubeck, T. G. Rauch, M. Weigand, E. Goering, M. Burghard, and G. Schütz, History-dependent domain and skyrmion formation in 2D van der Waals magnet Fe_3GeTe_2, Nat. Commun. **13**, 3035 (2022).

[33] J. Lee, J. Yun, Y. Lee, B. Tak Kang, J. Sung Kim, N. Haberkorn, and J. Kim, Magnetic domain study in Fe_3GaTe_2 ferromagnet with strong perpendicular anisotropy using magnetic force microscopy, J. Appl. Phys. **136**, 123905 (2024).

[34] L. Powalla, M. T. Birch, K. Litzius, S. Wintz, F. S. Yasin, L. A. Turnbull, F. Schulz, D. A. Mayoh, G. Balakrishnan, M. Weigand, X. Yu, K. Kern, G. Schütz, and M. Burghard, Seeding and emergence of composite skyrmions in a van der Waals magnet, Adv. Mater. **35**, 2208930 (2023).

[35] Y. Sun, M. T. Birch, S. Finizio, L. Powalla, S. Satheesh, T. Priessnitz, E. Göring, E. Knöckl, C. Kastl, A. Holleitner, K. Kern, M. Weigand, S. Wintz, and M. Burghard, Localized spin textures stabilized by geometry-induced strain in 2D magnet Fe_3GeTe_2, Adv. Mater. **37**, 2506279 (2025).

[36] G. Ma, R. Du, F. Lian, S. Bao, Z. Guo, X. Cai, J. Xiao, Y. Han, D. Zhang, S. Jiang, J. Huang, X. Wu, A. S. Mayorov, J. Wen, L. Wang, and G. Yu, Tailoring coercive fields and the Curie temperature via proximity coupling in WSe_2/Fe_3GeTe_2 van der Waals heterostructures, 2D Mater. **11**, 035020 (2024).

[37] D. S. Kim, J. Y. Kee, J.-E. Lee, Y. Liu, Y. Kim, N. Kim, C. Hwang, W. Kim, C. Petrovic, D. R. Lee, C. Jang, H. Ryu, and J. W. Choi, Surface oxidation in a van der Waals ferromagnet $Fe_{3-x}GeTe_2$, Curr. Appl. Phys. **30**, 40 (2021).